Simplified Hybrid Laminar Flow Control for the A320 Fin Aerodynamic and System Design. First Results

Geza Schrauf* and Heiko von Geyr†

DLR Institute of Aerodynamics and Flow Technology, 38108 Braunschweig, Germany

A flight test with a simplified HLFC system on the vertical tail plane of an A320 aircraft was performed in April/May 2018. The aerodynamic and system design is discussed and first results of the flight tests are presented.

Nomenclature

p	=	Pressure, Pa
w	=	Averaged suction velocity, m/s
i_H	=	Setting angle of the horizontal tail plane, degree
H	=	Flight altitude, ft
Re	=	Reynolds number
Re_{rr}	=	Roughness Reynolds number defined in [2]
β	=	Side slip angle, degree
δ	=	Rudder deflection angle, degree
μ	=	Viscosity. kg/(m*s)
ρ	=	Density, kg/m³

Subscripts:

q_c	=	Subscript 'c' denotes a quantity in a suction chamber
q_d	=	Subscript 'd' denotes a quantity in the plenum or duct
q_s	=	Subscript 's' denotes a quantity on the outer side of the microperforation
q_0	=	Subscript '0' denotes a reference quantity
q_∞	=	Subscript '∞' denotes a quantity in the oncoming freestream

Introduction

LAMINAR flow has the potential to significantly reduce the fuel burn of transport aircraft, because friction drag constitutes about half of the total drag of an aircraft in cruise [1]. Whereas for smaller aircraft, laminarity can be achieved passively by suitable profile shaping, active boundary layer control by suction is necessary for larger aircraft. For those aircraft, laminarity can be obtained by applying suction before the front spar in combination with a suitable shape of the wing box. The applicability of such hybrid laminar flow control (HLFC) systems was shown in the 1990s by flying with such a system, for example, on the wing of a Boeing 757 [2] and, later, on the vertical tail plane (VTP) of an A320 [3, Fig. 1]. A good overview of the technology status of that time, can be found in [4]. Because those suction systems were very complex, heavy, and difficult to manufacture, simpler and lighter systems needed to be developed to make hybrid laminar flow control (HLFC) feasible for commercial use.

A major step towards simplification was the "simplified suction system," already proposed by Horstmann and Schröder [5] in 2001 within the European ALTTA project. A sketch of this system is shown in Fig. 1. They replaced the complex suction system used in previous flight tests by a simple double skin structure. The outer skin is, as before, a microperforated titanium sheet which is supported by an inner sheet with stringers. According to Horstmann, the

---

*Research Scientist, DLR Institute of Aerodynamics and Flow Technology, Lilienthalplatz 7, 38108 Braunschweig, Germany, AIAA Senior Member.

†Head of Department, DLR Institute of Aerodynamics and Flow Technology, Lilienthalplatz 7, 38108 Braunschweig, Germany.
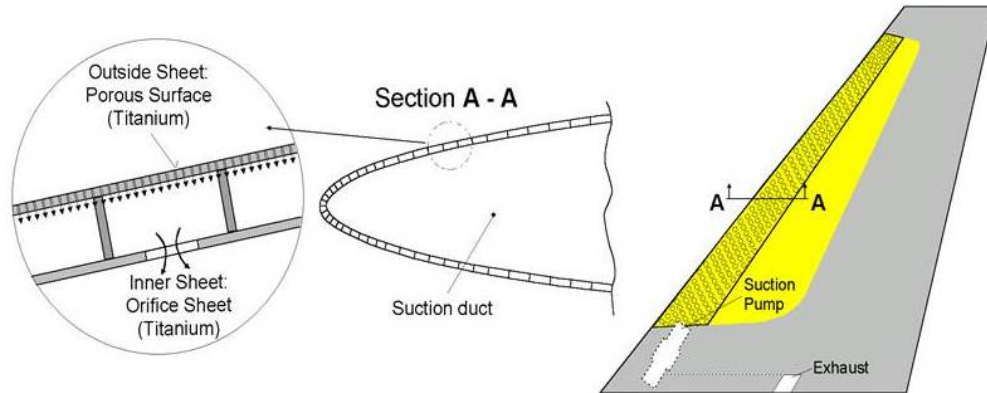
Fig. 1   Sketch of the simplified ALTTA system.

small compartments created by the stringers should also act as suction chambers. This can be achieved with the help of throttle orifices. Thus, the complex system consisting of suction chambers, tubes, and valves is no longer necessary and can be replaced by an empty space: the plenum or suction duct. The challenge of this concept is that we no longer have the option to control the suction with the help of valves. The microperforation, the stringer locations, and the throttle holes must be balanced so that sufficient suction is generated for all flight conditions. At that time, we could only show theoretical feasibility with numerical tools.

Fig. 2   Full-scale model of A320 VTP with refined simplified HLFC system in the DNW-LLF tunnel.

Much later, we were able to refine this concept as explained in Schrauf and von Geyr [3] and to build a full-scale wind-tunnel model of an A320 VTP presented in Fig. 2. In 2014, we could finally test this model in the Large Low-Speed Facility (DNW-LLF) in the Netherlands. The tests at realistic flight Reynolds numbers proved that simplified HLFC is not only theoretically possible, but can be realized in practice.

The next logical step was to aim for a flight test demonstration. The aerodynamic and system design of the flight test article will be decribed in this paper. Design and flight tests were performed within the European AFLoNext project.

2
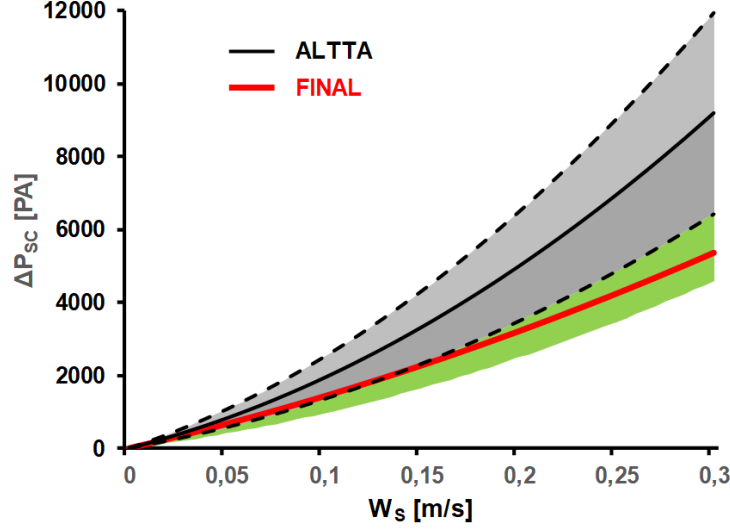
Fig. 3   Design range of pressure loss characteristics.

Design of the Simplified HLFC System for the A320 VTP

The simplified suction system for the flying article was of the ALTTA type, i.e. it contained a microperforated outer sheet which was supported by an inner sheet with the help of stringers. The stringers form small chambers or compartments inside of the microperforation. The sucked-in air is discharged into a plenum through throttle orifices in the inner skin. The art of the design is to match the microperforation with stringer distances and throttle hole size and number, so that sufficient suction is generated to suppress cross-flow transition for all flight conditions.

For this flight test, it was required that the suction system should be able to run in two modes, an active mode, driven by a compressor, and a passive mode, in which suction was generated with the help of a flap. The design range for the active mode is given in Table 1. For the passive mode, we relaxed the requirements for side slip and rudder angles to

Table 1   Design range for the HLFC system.

Flight altitude	H	$29000\,ft,\ 31000\,ft,\ \dots,39000\,ft$
Mach number	M	$0.76,\ 0.78,\ 0.80$
Side slip angle	β	$-2^0,\ -1^0,\ 0^0,\ 1^0,\ 2^0$
Rudder deflection angle	δ	$-2^0,\ -1^0,\ 0^0,\ 1^0,\ 2^0$

only ± 1 degree. Due to the symmetry of the VTP, we do not need to consider all possible combinations of the angles β and δ. It is sufficient to perform design calculations for the cases $(\beta = 0^0, \delta = 0^0)$, $(1^0, -1^0)$ and $(2^0, -2^0)^*$. For structural design, the case $H = 29000\,ft$, $M = 0.8$, $\beta = 2^0$ and $\delta = -2^0$ is the most critical one regarding pressure loads.

Microperforation

We simplified the design task by separating aerodynamic and system design from the manufacturing of the suction panel. This means that we do not consider any geometric properties of the microperforation, such as diameter, conicity, or pitch of the suction holes. However, we do assume that the microperforation can be described by a pressure-loss characteristic of the form[†]

$$\Delta p \ = \ A\,\frac{\mu_s}{\mu_0}\,w_s \ + \ B\,\frac{\rho_s}{\rho_0}\,w_s^2. \tag{1}$$

The initial values for the coefficients, $A = 13553\,kg/(m^2\,s)$ and $B = 56845\,kg\,s/m^3$, were taken from the ALTTA project [5]. We did not consider a single characteristic, but allowed for the gray range shown in Fig. 3. With this,

---

*The combination of positive side slip angle and negative rudder deflection angle produces the largest flow deflection. Alternatively, one could use opposite signs.

[†]The reference quantities are the values of the standard atmosphere at sea level, i.e. $\mu_0 = 1.792\,10^{-5}\,kg/(m\,s)$, and $\rho_0 = 1.225\,kg/m^3$.

we could work on the aerodynamic as well as on the system design of the HLFC system, requiring that the design should work for each pressure-loss characteristic in this range. In parallel, the producer of the microperforated panel began developing a stable manufacturing process, which would guarantee that the pressure-loss characteristic of the manufactured panel was within the same range. This task, however, was more difficult than anticipated, even with today's modern laser-drilling capabilities. The development of a stable process took several years, and the pressure-loss characteristic which could be reliably obtained was still slightly outside of the design range. Meanwhile, it has become clear that toleration levels for the A320 VTP microperforation were less stringent than originally thought. We found that we could expand the design range by including the green area with no adverse effect.

During the process development, several test samples were produced and their pressure-loss charactistics were measured with a laminar flow meter [10] developed for this purpose. The pressure-loss characteristic of the final suction sheet was measured by using test pieces made from left-over material. Finally, after the assembly of the HLFC leading edge, the microperforation was again checked with a portable flow meter developed for this purpose.

Details of the Suction Sheet

The suction sheet is made out of titanium with a thickness of $0.8mm$. The final values of the diameters of the suction holes are in the order of $55\mu m$ and the average hole distance is $565\mu m$. The final pressure-loss characteristic is shown as red line in Fig. 3. The values of its coefficients are $A = 12400\,kg/(m^2\,s)$ and $B = 18270\,kg\,s/m^3$.
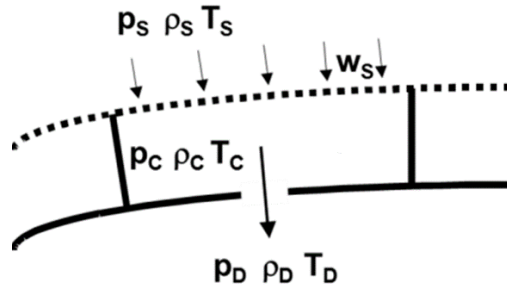
Fig. 4 Suction chamber and inner panel with a throttle hole.

Throttle Holes

The stringers and the inner sheet with the throttle orifices are also manufactured out of $0.8mm$ thick titanium plates. The inner sheet has throttle holes, as shown in Fig. 4, to generate sufficient suction in each small chamber and for each flight condition. We can determine the size and the number of throttle holes for each suction chamber with the help of the equation

$$\dot{m} \;=\; C \;\; A \;\; \sqrt{p_c\,\rho_c\;\frac{2\gamma}{\gamma-1}\;\left\{\left(\frac{p_d}{p_c}\right)^{2/\gamma} \;-\; \left(\frac{p_d}{p_c}\right)^{(\gamma+1)/\gamma}\right\}} \tag{2}$$

for the mass flow through one throttle orifice with cross section area A. This equation is an extension of the compressible Bernoulli equation [3, 6]. Herein, C is the discharge coefficient of the throttle orifice. As before, specimens with throttle holes of different sizes were drilled and their discharge coefficients were determined with the flow meter[‡].

It is a good practice to avoid throttle holes which are too small. Their discharge coefficients might exhibit large variations induced by small geometric irregularities of their edges. With larger holes, the influence of the edges is weaker. This is because the circumference of a hole increases linearly with the diameter, whereas its area increases quadratically, so that the ratio "circumference/area" becomes smaller.

[‡]Flache, B., and Seitz, A., "Discharge coefficients of orifice plates," private communication, 2016.
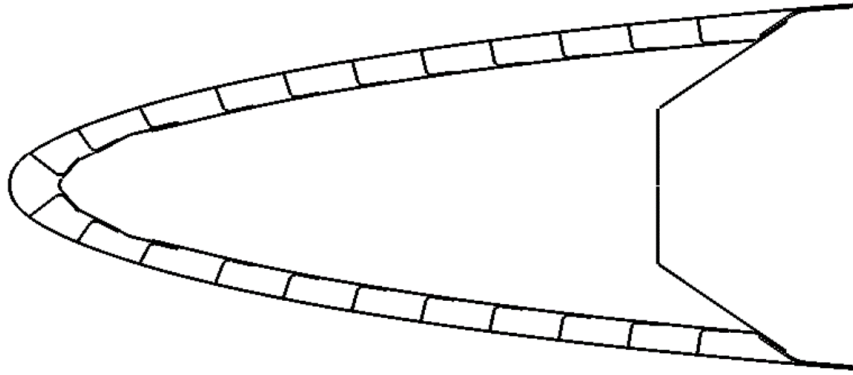
Fig. 5   Suction chamber Layout.

The mass flow through one chamber can be computed with equations (1) and (2). The equations for all chambers form a system with a special structure which can be solved with a fast algorithm [7]. This algorithm is implemented in the program SCDP [8], with which we calculated the suction velocities as input for the boundary layer computations.

Aerodynamic Chamber Design

The stringers between the microperforated outer and inner sheets have two functions: first, to provide structural stiffness and, second, to form small suction chambers. A sketch of this double skin is shown in Fig. 5. From the aerodynamic point of view, we have the following requirements on the stringer positions and on the microperforation:

1) Keep the attachment line laminar by satisfying the K-criterion [9]
2) No stringer should be positioned at the leading edge to allow for suction at the attachment line
3) Generate sufficient suction to delay transition
4) Allow for local blockage caused by stringer weld lines
5) Avoid outflow when flying with sideslip, because outflow triggers immediate transition
6) Avoid transition by "equivalent roughness," aim for Re_{rr} values below $400 - 450$ (cf. [2])
7) Avoid choking in the suction holes by keeping the Mach number of the hole flow below 0.3
8) Minimize mass flow and suction power
9) Aim for a robust design by allowing for a large variation of the pressure-loss characteristic of the microperforation

In the above list, requirements 1-5 are strict, meaning that if one of them is violated, laminarity is lost. Items 6 and 7 are good design guidelines, the given values can be relaxed.

To carry out the chamber design, we used the following numerical tools:

- 3D-RANS computations for the complete A320 configuration with the DLR-TAU code [13, 14]
- Grid generation with SOLAR using 81 million nodes
- Rudder deflection and HTP trim setting realized by grid deformation
- Suction velocities, stringer positions, and chamber flow calculated with SCDP [8]
- Boundary layer and stability calculations by COCO [15] and LILO [16]
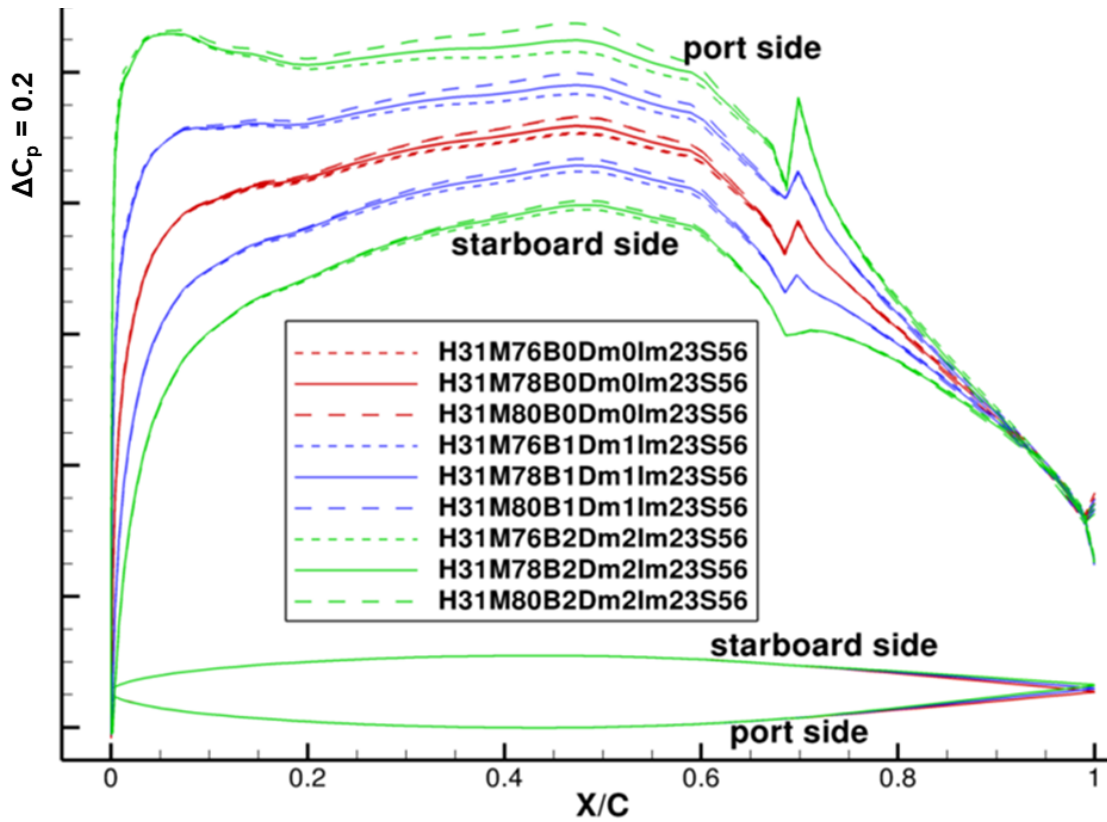
Fig. 6   Pressure distributions.

Details of Design

Next, we present some results from the design cycles. Fig. 6 shows pressure distributions for Mach numbers 0.76, 0.78, and 0.80, sideslip angles changing from 0^0 to 2^0 degrees, as well as rudder deflection angles 0^0, -1^0, and -2^0 degrees. We see that all pressure distributions have large gradients at the leading edge, limiting the size of the suction chambers in this region. Away from the leading edge, i.e. for $X/C > 0.05$, the pressure gradients are much smaller, so that from the aerodynamic point of view, only a few large chambers would be needed. Here structural requirements are driving the number and the positions of the stringers. Fig. 5 shows the final layout with twenty-three suction chambers.
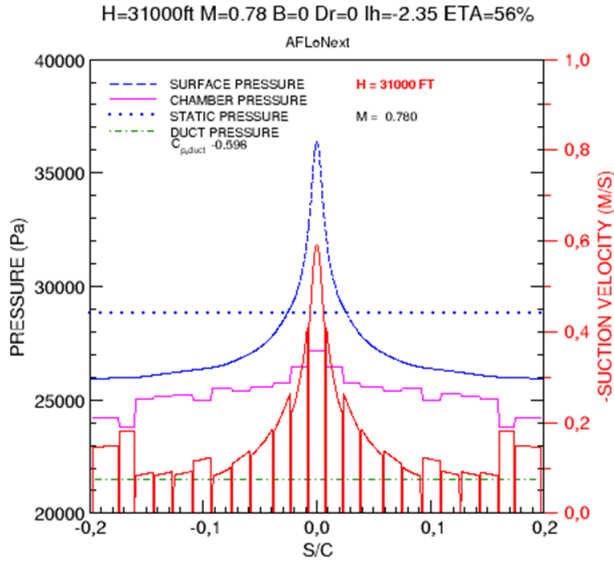
(a) Surface pressure, system pressures, and suction velocities.
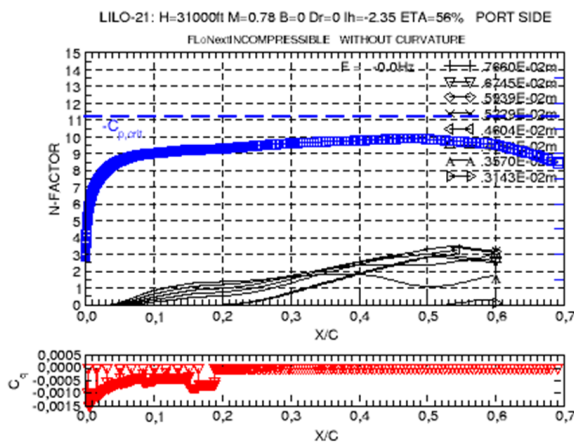
(b) N_{CF}-factors for the port side.
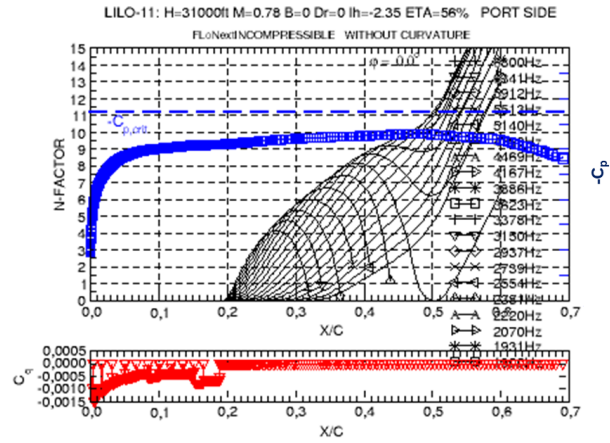
(c) N_{TS}-factors forthe port side.

Fig. 7   System pressures and N-factors for a symmetric case.

In Fig. 7a we present some results for a symmetric case with flight altitude $31000\,ft$, Mach number 0.78, and sideslip angle as well as rudder deflection angle 0°. The pressure along the outside surface is shown with the blue curve and the chamber pressures with the piecewise constant, pink one. Furthermore, we have, in red, the suction velocities generated by this pressure difference. We see that the suction velocity between two chambers is zero, due to the blockage of the weld line. The horizontal green line represents the plenum or duct pressure, which, in this case, is $21500\,Pa$.

The N_{CF}- and N_{TS}-factors are shown in Figs. 7b and 7c. As expected, suction limits the growth of the N_{CF}-factors and delays TS-growth until the end of the suction panel. Downstream of it, we observe strong growth of Tollmien-Schlichting waves leading to transition. Assuming a critical N_{TS}-factor of 9.5, we predict transition to occur at 43%.
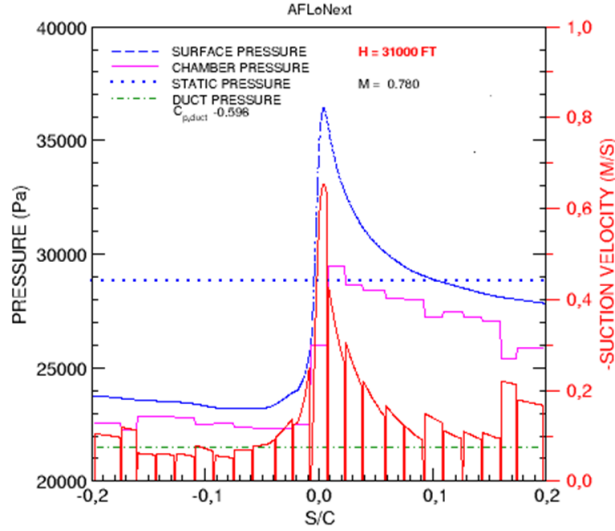
(a) Surface pressure, system pressures, and suction velocities.
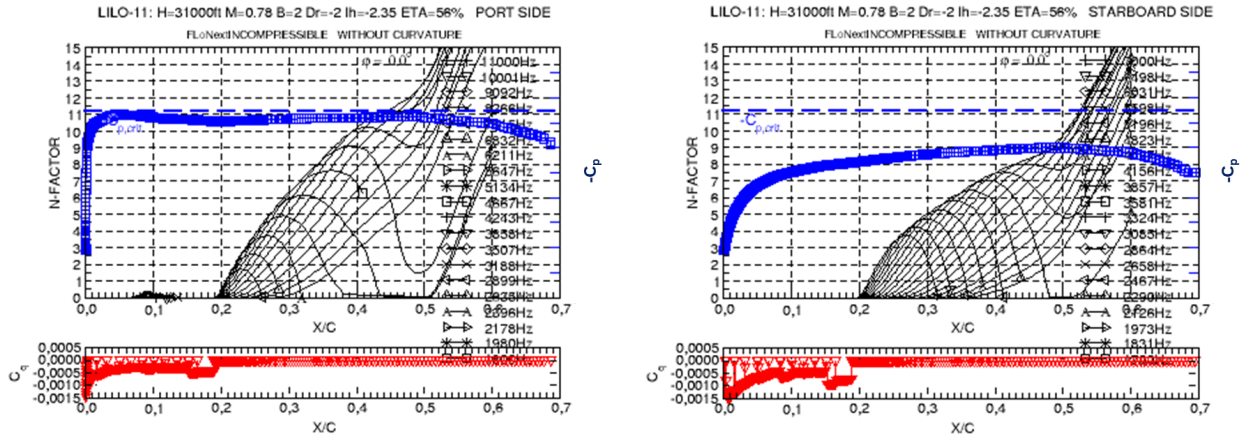
(b) N_{TS}-factors for port side.

(c) N_{TS}-factors for starboard side.

Fig. 8   System pressures and N-factors for an asymmetric case with two degrees sideslip.

In Fig. 8 we present a case at the same flight altitude, Mach number, and plenum pressure, however, this time with sideslip angle 2° and rudder deflection angle of -2°. This asymmetry is reflected in the pressure distribution (cf. Fig. 8a). We see that the difference between inside and outside pressure becomes very small at the port (left) side of the nose chamber around $S/C = -0.007$. A further increase of the plenum pressure or an enlargement of the nose chamber would cause flow reversal at this location, i.e. air would leave the suction chamber through the microperforation. This local outflow§ would cause the boundary layer to become turbulent. By reducing the sideslip angle, the pressure distribution becomes less asymmetrical as can be seen from Fig. 6. Thus, the difference between inside and outside pressure at $S/C = -0.007$ becomes larger, so that suction is still achieved for higher plenum pressures which can be generated with less power. This is why we relaxed the design requirements for passive suction: the suction power of a flap might be more limited than that of a compressor.

In Fig. 8b and 8c we present the N_{TS}-factors for both sides. We do not show the N_{CF}-factors because they are small. On both sides, transition is caused by Tollmien-Schlichting instability, at 38% on the port side and at starboard to 42%. We also observe a weak growth of Tollmien-Schlichting waves at $X/C = 0.1$ on the port side, resulting from the weaker suction at this location.

---

§We distinguish between local and global outflow. With local outflow, there is still suction over some parts of the chamber, whereas global outlow means outflow over the whole chamber.

Fig. 9   Suction flap on starboard side.

Flight Test Instrumentation

As mentioned before, the suction power for the HLFC system was to be generated in two ways. First, in an active mode, in which suction was generated with the help of an array of small, off-the-shelf compressors that were already certified for flight. In the second or passive mode, suction was generated with a flap on the starboard side, shown in Fig. 9, which could be opened and closed from the cabin.
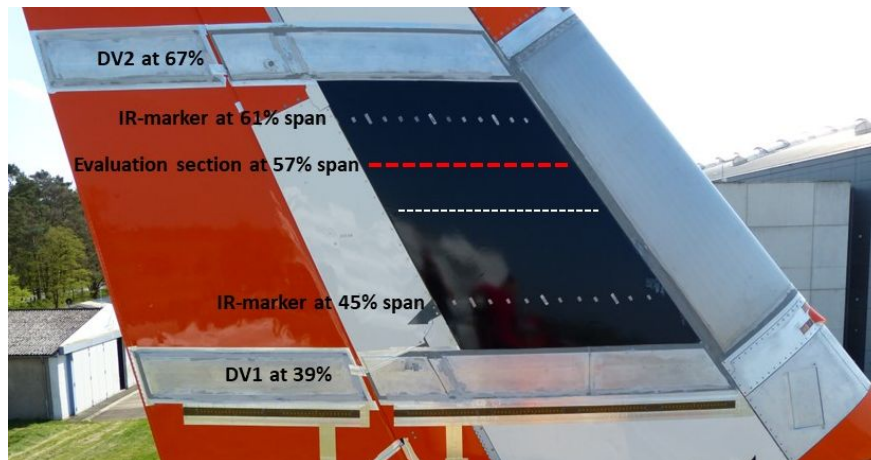
Fig. 10   Pressure sections DV1 and DV2 on starboard side.

The functionality of the suction system was verified with the following multitude of sensors:

- In each suction chamber with two classical pressure probes and with two MEMS sensors measuring temperature, pressure, and humidity, one at 25% and the other one at 75% span
- In the plenum or duct with two classical pressure probes and with two MEMS sensors measuring temperature, pressure, and humidity one at 25% and the other at 75% span
- A mass flow meter before the compressor, for active suction only
- Two sections with classical pressure taps: DV1 at 39% span and DV2 at 67% span (cf. Fig. 10)
- Two infrared cameras for simultanous transition detection on both sides of the VTP, installed in the horizontal tail plane (cf. Fig. 11)
- Hot film sensors to check the laminarity of the flow at the attachment line
- Additionally, a MEMS pressure belt on each side of the VTP box below DV1

9
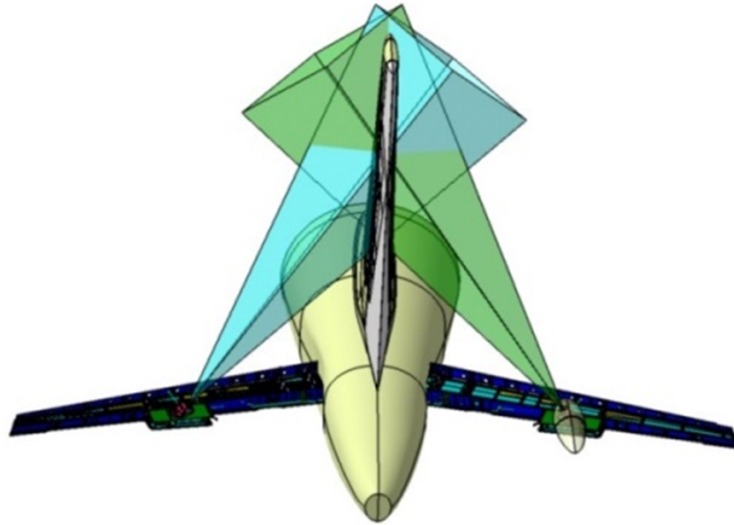
Fig. 11   Infrared cameras mounted in the horizontal tail planes.

Fig. 12   A320 aircraft with HLFC system installed in the VTP.

Fig. 12 shows the aircraft with the installed HLFC VTP on the tarmac at Brunswick airport.
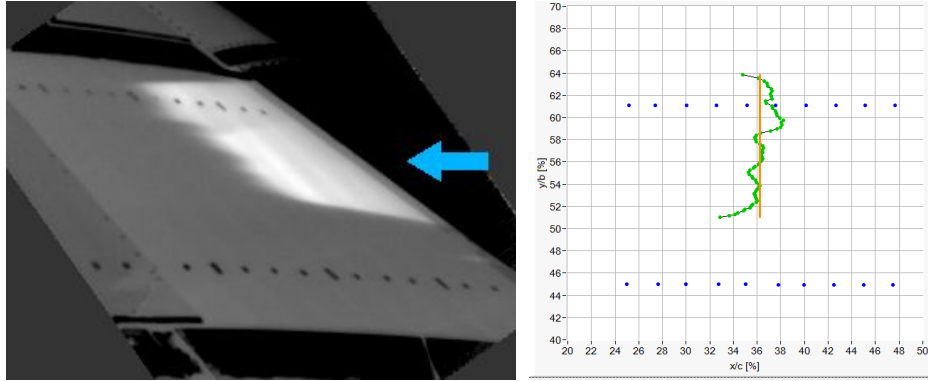
(a) Infrared image of starboard side.

(b) Transition line.
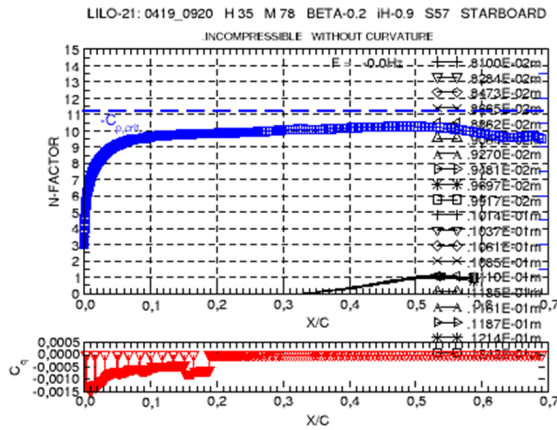
(c) N_{CF}-factors.
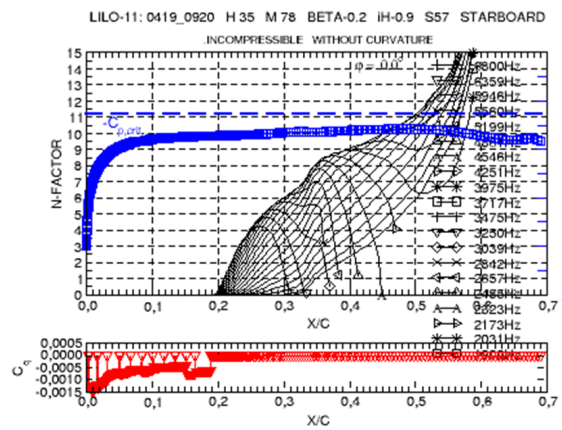
(d) N_{TS}-factors.

Fig. 13   Flight test measurement A.

First Flight Test Results

As a first result, we present measurement A, during which the aircraft was flying with Mach number 0.78 at altitude of $35000\,ft$. At the time at which the infrared image 13a was taken, the sideslip angle was β was -0.2^o and the rudder deflection angle -0.7^o, so that we can consider this case to be symmetric. The infrared image shows good contrast, because this side of the VTP was illuminated by the sun. The result of the image processing is shown in Fig. 13b with the green line indicating transition, which occurs between 36.5% and 38% chord in the spanwise range $0.56 < \eta < 0.59$. The transition line was obtained by an automated image processing and analysis tool, developed by DLR, to avoid any bias of human transition line determination.

The two plenum pressures at 25% and 75% span were $17061\,Pa$ and $17086\,Pa$, respectively, so that the spanwise pressure difference is only $25\,Pa$ or 0.15%. With the freestream pressure $p_\infty = 23840\,Pa$, we obtain a difference between the averaged plenum pressure and the freestream pressure of $6766\,Pa$, i.e. we have a case with strong active suction. The relative humidity of the air in the plenum was 5% so that the air was very dry.

In Figures 13c and 13d, we present the results of boundary layer and subsequent stability analysis with incompressible[¶] theory, performed at the spanwise section of 57%. Because of the strong suction, crossflow and Tollmien-Schlichting instabilities are completely damped over the suction panel. Further downstream, on the VTP box, we observe weak CF and strong TS amplification which then triggers transition. With a measured transition location of $0.365 < X/C < 0.38$, we obtain, correlated N_{TS}-factors between 8.5 and 8.8.

[¶]For transonic flow, we prefer N-factors computed with incompressible stability theory, because the N-factors obtained with compressible stability theory exhibit a larger Mach number dependence as shown in Atkin and Schrauf [17, Fig. 9]. The correlated compressible N_{TS}-factor would be in the order of 5.
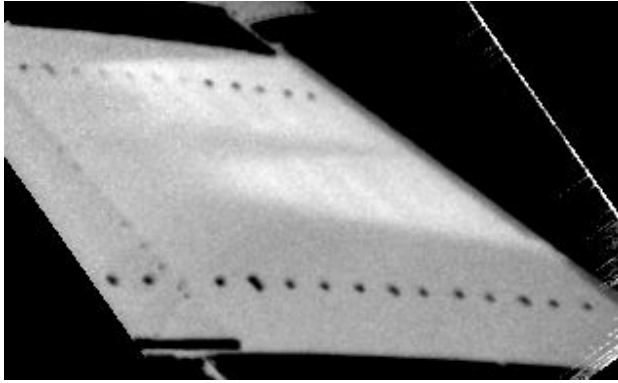
(a) Infrared image of starboard side.
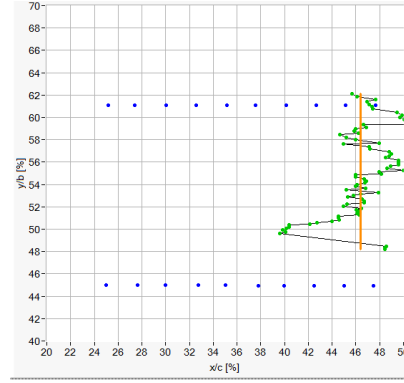
(b) Transition line.
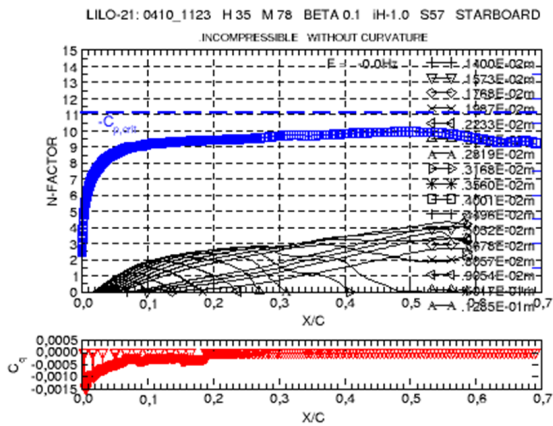
(c) N_{CF}-factors.
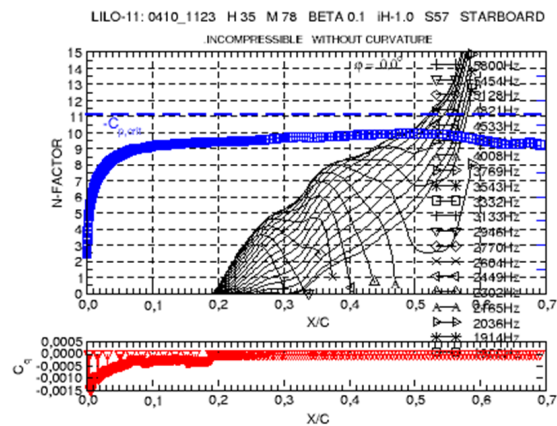
(d) N_{TS}-factors.

Fig. 14   Flight test measurement B.

Next, we present flight test measurement B which was also taken at flight altitude $35000 ft$ and Mach number 0.78. Sideslip and rudder deflection angles were 0.1^o and -0.4^o, respectively, i.e. we have again a symmetric case. This time, the starboard side was the shady side, so that the contrast in the infrared image is less pronounced. According to the image processing shown in Fig. 14b, transition occured between 48% and 50% in the spanwise range $0.56 < \eta < 0.59$. The plenum pressures were $19649 Pa$ and $19654 Pa$. The difference between averaged plenum and freestream pressure was only $3613 Pa$, i.e. much smaller than for the previous measurement. The effect of the weaker suction can be seen in Fig. 14c, showing some CF amplification‖ over the suction panel. Nevertheless, transition is still triggered by the Tollmien-Schlichting instability. The correlated N_{TS}-factors are $10.0 - 10.5$. They are somewhat larger than for measurement A. This might result from a somewhat lower surface temperature because, for this measurement, the starboard side was the shady side and it is known that surface heating provokes an earlier transition.

Outlook

Our results show that the HLFC system operated as expected in active and passive mode. The transition was delayed as predicted with our numerical tools.

We plan a follow-up paper with a detailed analysis of the flight tests based on boundary layer and linear stability theory.

‖Without suction, transition would be caused by the cross-flow instability very close to the leading edge, as is demonstrated in [3, Fig. 13].

Acknowledgments

References

[1] Schrauf, G., "Status and Perspective of Laminar Flow," *The Aeronautical Journal*, Vol. 109, No. 1102, 2005, pp. 639–644.

[2] Boeing Commercial Aircraft Group, "High Reynolds Number Hybrid Laminar Flow Control (HLFC) Flight Experiment II. Aerodynamic Design," NASA CR-1999-209324, April 1999.

[3] Schrauf, G., and von Geyr, H., "Simplified Hybrid Laminar Flow Control for Transport Aircraft," In: Eberhardsteiner J. et al. (eds), *European Congress on Computational Methods in Applied Sciences and Engineering (ECCOMAS 2012)*, 2012, Vienna, Austria.

[4] Braslow, A. L., "A History of Suction-Type Laminar-Flow Control with Emphasis in Flight Reserach," *Monographs in Aerospace History*, No.13, NASA History Division, 1999, Washington, DC.

[5] Horstmann, K. H., and Schröder, W., "A Simplified Suction System for a HLFC L/E Box of an A320 Fin," *ALTTA Technical Report*, No. 23, 2001.

[6] Idelchik, I. E., "Handbook of Hydraulic Resistance," Jaico Publishing House, Mumbai, 2003. English Translation from the second Russian edition, 1975.

[7] Keller, H. B., "Numerical Solutions of Bifurcation and Non-Linear Eigenvalue Problems." In Rabinowitz P. (ed.), *Application of Bifurcation Theory*. Academic Press, New York, 1977, pp. 359 -384.

[8] Schrauf, G. "SCDP – A Suction Chamber Design Program. Version 1.5," *GSSC Technical Report* No. 8.5, January 2015.

[9] Arnal, D., Juillien, J. C., Reneaux, J., and Gasparian, G., "Effect of Wall Suction on Leading Edge Contamination," *Aerospace Science and Technology*, No. 8, 1997, pp 505-571.

[10] Seitz, A., "Messkörper, Durchflussmesssystem und Computerprogramm dafür," Offenlegungsschrift DE 2015 113 999 A1 2016.03.03, Anmeldetag 24.08.2015, Offenlegungstag 03.03.2016, Deutsches Patent- und Markenamt.

[11] Boeing Commercial Airplane Company, "Hybrid Laminar Flow Control Study. Final Technical Report," NASA/CR-1982-165930, October 1982.

[12] Schrauf, G., "SHR – A Program to Check the Suction Hole Requirements. Version 2.0," *GSSC Technical Report* No. 9, April 2016.

[13] "TAU-Code User Guide," Release 2007.1.0, Institute of Aerodynamics and Flow Technology, German Aerospace Center, April 2007.

[14] Schwamborn, D., Gerhold, T., and Heinrich, R., "The DLR TAU-Code: Recent Applications in Research and Industry," In: Wesseling P., Oñate E., and Périaux J. (eds.), *European Conference on Computational Fluid Dynamics, ECCOMAS CFD 2006*, Egmond aan Zee, The Netherlands, 5-8 September 2006, CD-Rom Proceedings, ISBN: 90-9020970-0, TU Delft,The Netherlands.

[15] "COCO - A Program to Compute Velocity and Temperature Profiles for Local and Nonlocal Stability Analysis of Compressible, Conical Boundary Layers with Suction," *ZARM Technik Report*, November 1998.

[16] Schrauf, G., "LILO 2.1 User's Guide and Tutorial," Bremen, Germany, *GSSC Technical Report* No. 6, originally issued 2004, modified for Version 2.1 July 2006.

[17] Atkin, C., and Schrauf, G., "Progress in Linear Stability Methods for Design Applications," ECCOMAS 2000, 11-14 September 2000, Barcelona, Spain. CD-ROM Proceedings by ECCOMAS, ISBN: 84-89925-70-4.